Interdisciplinary Studies on Applied Science, 3(1):38–48, 2026. DOI: 10.58613/isas314

Interdisciplinary Studies on Applied Science

Journal homepage: https://www.gpub.org/journal-details.php?journal-id=42

ISSN (E): 3048-877X

Research Article

Vibrational Spectroscopic Analysis and Laser Irradiation Effect on Pharmaceutical Compounds: An Integrated Experimental and Density Functional Theory Approach

Zainab A. Elzahra [1*]

[1] *Department of Vision Screening Techniques, College of Health and Medical Techniques, Al-Furat Al-Awsat Technical University, An-Najaf, Iraq.*

[*] *Corresponding author: zainab.hassanchm@atu.edu.iq*

Article Info

Keywords: *Vibrational Spectroscopy, Raman Scattering, Density Functional Theory, Laser Irradiation, Photodegradation, Chemometrics, Pharmaceutical Stability, FTIR Analysis.*

Received: *30.01.2026;*
Accepted: *24.02.2026;*
Published: *02.03.2026*

Abstract

Knowledge of structural integrity of pharmaceutical compounds at energetic stress is essential to drug safety and efficacy. The paper describes a detailed experiment on the molecular stability of active pharmaceutical ingredients under constant wave laser light, which is performed with the help of a unified system of vibrational spectroscopy and quantum mechanical simulations. The vibrational landscape of the target compound was mapped using high-resolution Raman scattering and Fourier Transform Infrared spectroscopy and a solid theoretical basis of spectral assignment was presented using Density Functional Theory at a B3LYP/6-311++G(d,p) level. The geometry at the ground-state was determined with great accuracy by correlation of experimental mode measurements and calculated potential energy distributions. Dose dependent spectral changes with effects of exposure to 532 nm laser excitation included the destruction of the aromatic ring breathing mode at 1000 cm^{-1} and the appearance of a specific redshift in the carbonyl stretching vibration. These spectral changes indicate that the mechanism is important in the disruption of intermolecular hydrogen networks and local photochemical disordering as opposed to direct thermal decomposition. Latent statistical analysis of the spectral data showed that the Principal Component Analysis was useful in separating native and irradiated samples on the basis of variation in individual vibrational bands. The results prove that experimental spectroscopy fingerprints coupled with theoretical modeling provide a robust methodology of non-destructive monitoring of the photodegradation profiles of sensitive pharmaceutical materials.

1. Introduction

Vibrational spectroscopy is one of the separate strongholds of the contemporary physicochemical analysis that provides unique information about the molecular structure and dynamic behavior of chemical substances. Raman scattering and Fourier Transform Infrared (FTIR) absorption are techniques that give specific molecular fingerprints that can be used to identify chemical bonds, functional groups and crystalline structures with great accuracy. Use of such techniques is not limited to the identification process; spectral data is an important part of quantitative analysis and structural explanation of complex pharmaceutical matrices. The most recent concepts of quantum mechanical simulations in conjunction with experimental spectral data have transformed the knowledge of molecular vibrations. Studies [1] reveal that application of low-frequency vibrational spectroscopy with quantum mechanical modeling can be useful in describing crystalline polymorphs

of antiviral substances. They can be used to assign spectral features without ambiguity, to attain a difference between subtle conformational differences which could be obscure with experiment data alone.

The significance of the awareness of the molecular stability in different stress conditions cannot be overrated. The change that occurs to pharmaceutical compounds and biological molecules when subjected to external sources of energy such as lasers or ionizing radiations are very dramatic in terms of the structural changes. In the study [2], the vibrational spectra with Density Functional Theory (DFT) calculation were used to discuss the molecular structure of pharmaceutical cocrystals, and it was proved that the theoretical modelling can give the required validation to the experimental results. These changes can only be precisely characterized with an excellent analytical structure. Vibrational spectroscopy aids in tracking of breaking of bonds, creation of new chemical species and transformation in energy of the lattice. It is also pointed out that additional research on solvent effects and structure of complex antibiotic solvates is being attempted by the use of value of molecular spectroscopy in conjunction with DFT studies [3]. All the studies have the same foundation of the concept of integrated approach in which the experiment and theory intertwine and explain the physical phenomena.

Vibrational fingerprinting in the medical and biological fields has passed out of laboratory exaltation to clinical requirement. Expansive coverage [4] narrates that, in evolution of vibrational spectroscopy, expansion has been achieved of the ability to detect pathological changes in tissues, since development of vibrational spectroscopy into clinical practice. This translational performance is based on the infrared and Raman mode sensitivity to biochemical changes. Proteins, which are basic components of biological equipment, have unique infrared patterns. Details of protein infrared spectroscopy [5] elaborate how the amide bands can be used to derive information on the secondary structure that is essential when evaluating radiation-induced denaturation or aggregation.

Reliability of data in the spectroscopic analysis relies on strict processing and standardization. Chemometrics harmonization of Raman spectroscopy will guarantee that the spectral data is comparable when comparing instruments or laboratory experiments [6]. In the absence of this standardization subtle spectral changes caused by the irradiation with a laser would be misconstrued as inartificial artifacts of the instrument instead of chemical changes. What is more, biological samples tend to pose such issues as light scattering. It is possible to obtain pure absorption spectra of a highly scattering biological sample by applying the correction method of Resonant Mie Scattering (RMieS) [7] that guarantees that observed spectral changes are due to biochemical changes, rather than to scattering effects.

The radiations impacting the biological and pharmaceutical systems pose a challenging task which demands high-level detection technologies. Recent studies [8] examined application of Raman spectroscopy with covariate-adjusted multivariate analysis in the detection of irradiated blood and the study showed high sensitivity of the vibrational modes to radiation-induced oxidative stress. X-ray irradiation causes certain chemical modifications in the nuclear and membrane areas at the cellular level. A study [9] examining neuroblastoma cells found that Raman micro-spectroscopy is capable of spatially resolving the damage in single cells, being able to differentiate between nuclear DNA damage and oxidation of membrane lipids.

Energetic disturbance can be experienced especially with nucleic acids. Previous FTIR experiments [10] defined spectral indicators of nucleic acid damage in terms of individual changes in phosphate backbone and base pairing vibrations. Multidimensional data processing is necessary to derive meaningful information of such complex data sets. Processing methods of Raman and infrared spectroscopy [11] review indicates a need to use advanced algorithms to isolate signal and noise and overlapping bands. The state of art techniques in computational algorithms, including convolutional model-based signal denoising [12] can further boost signal-to-quality ratio such that tiny spectral variations caused by low dose radiation or laser can be detected.

Basic aspects of the Raman techniques are still developing. State-of-the-art modes of Raman spectroscopy [13] are now available that can investigate nanoscale processes, which is essential in the study of the dynamic processes of laser energy dissipation in a crystal lattice cell or a biological cell. Experimental parameters are related to choice of outcome. The optimization of sample substrate and laser wavelength [14] is important in order to reduce the background of fluorescence and degradation of the sample, particularly in the case of working with sensitive biological specimens. It is especially important in the case of lipid peroxidation which is a process frequently induced by irradiation. The gamma-irradiation and UV-light induced lipid peroxidation have been successfully characterized using Fourier transform-infrared absorption studies [15], as the alteration of spectral changes attributable to the oxidative byproducts.

Spectral data must be classified with powerful statistical schemes. It is possible to compare PCA-LDA and PLS-DA methods [16] and assume that in terms of categorizing vibrational spectra of treated versus control samples, certain algorithms work better to provide good discrimination. This type of classification is essential in assessment of radiobiological sensitivity.

Normal human breast cell study [17] employed the Raman spectroscopy to monitor the radiobiological sensitivity as a time series to detect both transient and permanent spectral features of proton beam exposure. The knowledge of these markers in the biological models is applied to the study of drug stability because the processes of radical formation and bond scission are similar physicochemically.

Radiation molecular biology is seen in the context of history. Identification of radiation-damaged products was grounded on early infrared spectroscopy [18] of DNA bases. The development of synchrotron radiation sources has also made it possible to monitor online the damage caused by the X-ray in DNA [19] in a way that demonstrates that the damage can occur on timescale even viewable by real-time spectroscopy. The non-invasive diagnostic potential is currently afforded to label-free.

Raman micro-spectroscopy [20], which predicts damage and chromosomal radio sensitivity of DNA in peripheral blood mononuclear cells.

The versatility of Raman spectroscopy in the biological tissues [21] and FTIR in the tissue analysis [22] is provided by broad use of the techniques. They offer non-destructive ways in investigating sample integrity. Applications The spectral signature Applying spectral signatures to biological outcomes in cancer research, label-free Raman spectroscopy has demonstrated the signature of radiation resistance in tumor microenvironment [23]. On the contrary, lasers with high intensity themselves may cause degradation of the sample. The state of the art [24] on single living cells has shown that short wavelengths induce more serious photodamage when compared to near-infrared wavelengths, which is a parameter that needs to be regulated when performing stability testing on pharmaceuticals.

Complex cascade of biochemical alterations detectable by Raman micro-spectroscopy are the results of Subcellular response to X-rays [25]. Such changes are reminiscent of structural alterations in the isolated, double-stranded DNA [26] wherein the FT-Raman spectroscopy is used to detect strand breaks and base damages. The dosimetric tool is the monitoring of the dosing of therapeutic doses of gamma irradiation [27], which show dose-dependent changes in spectral alterations. Different spectral footprint is also left by proton irradiation. Investigations of the calf thymus DNA [28] and serum albumin [29] in proton and gamma irradiation demonstrate that secondary protein structure and stacking of DNA bases are very sensitive targets.

It has been stressed in reviews of biological tissue spectroscopy [30] that the vibrational modes of lipid, proteins, and nucleic acids overlap, and requires an integrated experimental and theoretical approach in order to pull out the contributions. Radiation damage of biomimetic models, e.g. lysozyme [31], is used to get simplified system used to check spectral assignments before using them in complex cells. Low irradiation levels also modify lipid domains in membranes [32], which are detected using Raman spectroscopy to show changes in chain order and packing. The ionizing radiation is used on specific populations of the lipid-protein interfaces [33], which reduces the membrane fluidity and functionality.

Combination of Density Functional Theory (DFT) and such experimental observations is used to overcome the shortcomings of empirical assignment alone. Although experiment demonstrates that a change has taken place, DFT calculations can be used to describe why it took place by simulating the redistribution of the electron density and potential energy surfaces. The combined method enables the separation of the thermal effects caused by laser and direct photochemical cleavage of the bond.

2. Literature Review

Numerous records about the use of vibrational spectroscopy in the investigation of radiation and laser energy impact on molecules are found in scientific literature. Studies lay much emphasis on identifying the tiny chemical changes that are caused by the absorption of energy. Literature review shows that three major directions exist: the pharmaceutical and crystalline structures have been characterized based on DFT, radiation-induced damage in biological macromolecules has been analyzed, and chemometric approaches to data interpretation have been developed.

Structural confirmation Structural confirmation can be done rigorously with the aid of Density Functional Theory (DFT) and experimental spectroscopy. The low-frequency vibrational spectroscopy was applied in investigations [1] involving antiviral drug ribavirin in order to distinguish crystalline polymorphs. Theoretical simulations in this experiment allowed assigning low energy phonon modes, which are vulnerable to intermolecular forces and lattice structures. In line with this, pharmaceutical cocrystals analysis [2] used DFT to analyze vibrational spectrums, which guaranteed proper mapping of hydrogen bonding networks in crystal lattice. Generalization of this technique to antibiotic solvates [3] established that solvent molecules in crystal structure have a strong effect on vibrational mode, which is well described by quantum mechanical calculations.

Radiation effects of nucleic acids and proteins make up a significant part of spectroscopical literature. DNA damage is still dominant theme. Infrared spectroscopy was used early [18] to catalogue photoproducts of DNA bases. They were followed by work by FTIR to determine the marker bands of oxidative damage on nucleic acids that reportedly observed the changing phosphate symmetric stretching vibrations. The effects of proton and gamma irradiation were also explained in the case of calf thymus DNA [28] and serum albumins [29] in which Raman spectroscopy detected dose-dependent decreases in the intensity of bands related to DNA backbone and protein amide linkages. Base unstacking and backbone scission were evidenced by structural changes in the structure of double-stranded DNA [26] studied using FT-Raman spectroscopy.

Another important area is the lipid and membrane damage. A study [15] had shown that FTIR was useful in the monitoring of lipid peroxidation caused by gamma and UV radiations. Analysis of the spectrum showed that carbonyl groups were formed and the unsaturation of fatty acid chains was lost. Even low-level irradiation experiments [32] of model membranes showed that lipid domain structure is altered by even the smallest amount of energy input. The study of the erythrocyte membranes [33] identified the presence of certain protein-lipid interactions as targets of the ionizing radiations.

There is macroscopic look of the molecular damage provided by cellular and tissue-level responses. Laser induced cell destruction thresholds were determined by Raman microspectroscopy [24], which pointed to experimental dependence on wavelength of phototoxicity. The high time resolution of Raman spectroscopy to monitor the temporal change in the cellular damage was shown by the analysis of neuroblastoma cells [9] and normal breast cells [17] which were subjected to X-ray beams and proton beams respectively. Label-free Raman has been used to successfully detect the signatures of radiation resistance in tumor environments [23] and therapeutic response in tumor environments [27]. Sub cellular spectral variations with lipid accumulation and protein phosphorylation were observed in prostate cancer cells that had been subjected to clinical levels of X-rays [25].

The development of methodology makes it easier to extract credible data using complicated spectra. General discussions on the usage of Raman [21] and FTIR [22] in tissues prepare the ground in understanding of biological spectra. Clinical diagnostics [4] is connected to molecular fingerprinting by comprehensive overview. Artifacts are minimized by optimization of experimental parameters such as the choice of substrates and laser wavelength [14]. Spectral clarity is improved by using sophisticated data processing [11] and denoising algorithms [12]. Reproduction is guaranteed by correction schemes to remove scattering [7] and standardization schemes [6].

Statistical classification techniques [16] like PCA and PLS-DA are essential for discriminating between irradiated and non-irradiated samples. Recent applications [8, 20] employ these multivariate methods to predict DNA damage in blood samples with high accuracy. Frontiers of technique [13] continue to expand, offering higher resolution and sensitivity where Table 1 summarizes key findings from selected studies, categorized by target material and radiation.

Integration of findings from biomolecular damage studies [5, 19, 30] with pharmaceutical structural analysis suggests that mechanisms of energy dissipation observed in biological tissues apply to solid-state pharmaceuticals. Synchrotron-based monitoring [19] proves that damage occurs on timescales relevant to laser interaction. Therefore, combination of experimental spectroscopy, whether Raman or FTIR, with theoretical verification via DFT constitutes most robust approach for predicting stability of compounds under irradiation.

Table 1: Summarizes key findings from selected studies, categorized by target material and radiation source.

Study Focus	Ref	Target Material	Radiation/Source	Key Findings using Spectroscopy
Crystalline/ Drug Structure	[1]	Ribavirin Polymorphs	N/A (Characterization)	DFT confirmed low-frequency modes assigned to lattice vibrations.
	[2]	Ethenzamide Cocrystals	N/A (Characterization)	Hydrogen bond networks elucidated via combined DFT and spectral analysis.
	[3]	Azithromycin Solvate	N/A (Characterization)	Solvent effect on vibrational modes validated by quantum calculations.
DNA/ Protein Damage	[28]	Calf Thymus DNA	Proton & Gamma	Dose-dependent intensity decrease in DNA backbone bands.
	[29]	Serum Albumin	Proton & Gamma	Changes in Amide I/III bands indicating secondary structure loss.
	[26]	dsDNA	Radiation	Identification of base unstacking and backbone scission markers.
	[31]	Lysozyme	Radiation	Radical-induced damage observed in biomimetic model system.
Cellular Response	[17]	Breast Cells (MCF10A)	Proton Beam	Time-resolved spectral markers of radiobiological sensitivity.
	[25]	Prostate Cancer Cells	X-rays	Subcellular mapping revealed lipid accumulation and protein changes.
	[9]	Neuroblastoma Cells	X-rays	Discrimination between nuclear damage and membrane oxidation.
	[24]	Living Cells	Laser (514 vs 660 nm)	Shorter wavelengths cause immediate photodegradation of samples.
Lipid/Membrane	[15]	Lipids	Gamma & UV	FTIR detected carbonyl formation indicating peroxidation.
	[32]	Model Membranes	Laser	Modification of lipid domain order observed at low energy levels.
Methodology	[8]	Blood	Ionizing Radiation	Multivariate analysis detected oxidative stress markers in liquid biopsy.
	[16]	Spectral Data	N/A (Analysis)	PCA-LDA and PLS-DA comparison for optimal classification accuracy.

3. Methodology

3.1. Materials and Reagents

Pharmaceutical grade active ingredients utilized in this study were obtained from Sigma-Aldrich with purity exceeding 99%. Solvents including methanol, ethanol, and acetone were analytical grade. Potassium bromide (KBr) for infrared spectroscopy was spectroscopic grade, dried at $110^{\circ}C$ for 48 hours prior to use. Silicon wafers used for Raman calibration were standard $< 100 >$ orientation. Deionized water with resistivity 18.2 MΩ·cm generated from Milli-Q system served for all aqueous solution preparations. No further purification of commercial reagents performed unless specified.

3.2. Sample Preparation

Solid-state samples were prepared to ensure homogeneity and reproducibility of spectral data. For Raman spectroscopy, crude pharmaceutical powder was recrystallized from methanol to obtain uniform micro-crystals. Crystals were gently ground using an agate mortar and pestle to reduce particle size effects and minimize scattering anisotropy. The resulting fine powder was packed into a circular aluminum sample holder with 2 mm depth. A glass slide was used to make the surface smooth so that the focal distance is consistent when exposing the laser.

In the Fourier Transform Infrared (FTIR) spectroscopy, the KBr pellet technique was used. The sample: KBr ratio was taken at 1:100 by weight. A 2-minute homogenization of the mixture was done using a vibrational mill in order to get a uniform mixture. The hydraulic pressure of 10 ton was applied on the powder mixture and allowed to rest under vacuum (5 minutes) to drive out trapped air.

Transparent pellets of about 1 mm in thickness and 13 mm in diameter were obtained as control pellets with pure KBr to obtain background spectra. Solvatochromic studies of liquid samples were conducted by dissolving the compound in different solvents with different polarities. The solution was introduced into a liquid cell using calcium fluoride (CaF_2) cell windows and a spacing of 0.05 mm.

3.3. Laser Irradiation Protocol

The variable continuous wave (CW) lasers with varying wavelengths were used to irradiate to investigate the energy-dependent molecular response. These were sources of a diode-pumped solid-state (DPSS) laser at 532 nm (green) and a diode laser at 785 nm (near-infrared) and Nd:YAG laser at 1064 nm. The samples were attached on a motorized XYZ translation stage. The microscope objective was a 10x focus on the sample surface to focus the laser beam. The size of the spot was measured with the help of the knife-edge method.

The neutral density filters were used to control the power density at the sample surface and a calibrated power meter was used to measure the power density. Exposure time was between 10 seconds and 60 minutes. Fluence (F) was calculated in order to measure the amount of

energy reaching the sample. It is a parameter that is a combination of power density with exposure time.

$$F = \frac{Pt}{\pi w_0^2}$$

where
P is the laser power in Watts; t is the time of exposure of the laser in seconds and w_0 is the beam waist radius in centimeters. To eliminate photochemical degradation and to identify the photothermal effects, temperature changes throughout the irradiation process was monitored with a non-contact infrared thermometer. Low-power experiments were done at ambient temperature $(25°C)$. Experiments with high power had a Peltier cooling stage that kept the base temperature constant.

3.4. Raman Spectroscopy Data Acquisition

Raman spectra were collected using a confocal micro-Raman spectrometer equipped with a liquid-nitrogen-cooled charge-coupled device (CCD) detector. The spectrometer system employed holographic notch filters to reject the Rayleigh scattering line. A grating with 1200 grooves/mm was selected to achieve a spectral resolution of 2 cm^{-1}. Calibration of the wavenumber axis was performed daily using the silicon phonon mode at 520.7 cm^{-1}.

Spectra were recorded over the range 50-4000 cm^{-1}. Accumulation time was set to 30 seconds with 5 averages to improve the signal-to-noise ratio (SNR). Cosmic ray removal was applied automatically during acquisition. Laser power at the sample was kept below 5 mW for non-destructive characterization scans. For degradation studies, power was increased stepwise. The geometry of scattering collection was a 180° backscattering configuration. The numerical aperture of the objective lens was 0.25. Depth profiling was performed by adjusting the Z-axis focus in 1 μ m increments.

3.5. FTIR Data Acquisition

Infrared spectra were acquired using an FTIR spectrometer equipped with a deuterated lanthanum α-alanine doped triglycine sulphate (DLATGS) detector. The optical path was purged with dry nitrogen gas to eliminate water vapor and carbon dioxide interference. Spectra were collected in transmission mode for KBr pellets and in Attenuated Total Reflection (ATR) mode for neat powders. The ATR accessory utilized a diamond crystal with a single reflection geometry.

Parameters were set to 64 scans per spectrum with a spectral resolution of 4 cm^{-1}. Interferogram apodization utilized a Blackman-Harris 3-term function. A zero-filling factor of 2 was applied to improve digital resolution. A background spectrum of an empty chamber or a clean ATR crystal was collected prior to every sample measurement. The ratio of the sample single-beam spectrum to the background single-beam spectrum yielded the transmittance spectrum. Absorbance was calculated as the negative logarithm of transmittance.

3.6. Computational Details: Density Functional Theory (DFT)

Quantum mechanical calculations were performed to aid spectral assignment and understand electronic structure changes. The Gaussian 09 software package was utilized for all simulations. The molecular structure was built using the GaussView visualization interface. Geometry optimization was carried out in the gas phase and with an implicit solvent model (PCM) to mimic experimental conditions.

The hybrid functional B3LYP (Becke, 3-parameter, Lee-Yang-Parr) was chosen because it has previously demonstrated its accuracy in the prediction of vibrational frequencies of organic molecules. It was based on the basis set 6-311++G(d,p) which was used to model valence electrons and add diffuse and polarization functions, which are important concepts in hydrogen bonding and lone pair interactions. Convergence criteria for geometry optimization were set to "Tight" limits. The absence of imaginary frequencies in the vibrational analysis confirmed a ground state energy minimum.

The total energy of the system in the DFT formulation is expressed as a functional of the electron density ρ(r).

$$E[\rho] = Ts[\rho] + \int V_{ext(r)\rho(r)dr} + \frac{1}{2}\frac{\int \rho(\mathbf{r})\,\rho(\mathbf{r}')}{|r-r'|dr} \times dr' + E_{xc}[\rho]$$

The terms represent the kinetic energy of non-interacting electrons (T_s), external potential energy (V), classical Coulomb repulsion (Hartree energy), and exchange-correlation energy (E_{xc}).

Calculated harmonic vibrational frequencies typically overestimate experimental values due to the neglect of anharmonicity and electron correlation approximations. A scaling factor was utilized to correct this systematic error. The B3LYP/6-311++G(d,p) level of theory was scaled by 0.967.

3.7. Data Pre-processing and Chemometric Analysis

The raw spectral data was exported to python and Origin Pro to be post-processed. Pre-processing involved quantizing-premedian averaging, smoothing and averaging. An asymmetric least squares algorithm was used to eliminate baseline drift. A Savitzky-Golay filter of 2^{nd} order polynomial with 9-point window was used to decrease high-frequency noise.

In order to compare normalization of spectra with different absolute intensities, normalization is required. The Standard Normal Variate (vector normalization) was used to normalize the samples considering the difference in the thickness of the samples and the packing density.

$$x_{norm} = \frac{x_i - x}{\sqrt{\sum (x_i - x)^2}}$$

Where x_i is spectral intensity (at a given wavenumber) and x is mean spectral intensity. To detect the trends in spectral data and differentiate between unirradiated and control samples, Principal Component Analysis (PCA) was used to select trends in spectral data. The spectral data

were mean-centered and the covariance matrix of the data was obtained. The covariance matrix produced principal components (PCs) using Eigenvectors. The parameters and settings of the computations applied during the study are summarized in Table 2.

Table 2: Experimental and Computational Parameters

Parameter	Raman Spectroscopy	FTIR Spectroscopy	DFT Calculation
Source/Functional	532 nm / 785 nm	Globar (Mid-IR)	B3LYP
Detector/Basis	CCD (-70°C)	DLATGS	6-311++G(d,p)
Resolution	2	4	Tight Convergence
Scans/Steps	5 acc 30 sec	64 scans	Optimization + Freq
Range	50-4000	400-4000	Full Spectral Range
Correction	Baseline / Cosmic Ray	Atm. Comp. / ATR	Scaling Factor 0.967

Root Mean Square Deviation (RMSD) was used to measure the conformity of the experimental (ν_{exp}) and the calculated (ν_{calc}) frequencies.

$$\mathrm{RMSD} = \sqrt{\frac{1}{N}\sum_{i=1}^{N}\left(\nu_{exp,i} - \nu_{calc,i}\right)^2}$$

A smaller value of RMSD is a sign of greater precision of the computational model. The visual animation of vibrational modes in Gauss View was assigned and compared with the potential energy distribution (PED) analysis in VEDA software.

4. Results

4.1. Molecular Geometry and Structural Validation

Density Functional Theory optimization of geometry gave the lowest energy structure of the pharmaceutical compound. Optimized bond lengths and bond angles were contrasted with available literature X-ray diffraction (XRD) data in order to confirm the theoretical model. There was good correlation of the gas-phase calculated structure with the experimental crystal structure in the solid state. Minor differences were explained by crystal packing forces in the XRD data that were not observed in the gas-phase DFT results.

The structure of the optimized structure is analyzed to demonstrate how aromatic rings are planar and the side chains are oriented in a particular way. Hydrogen bonds intramolecularly were determined through the distance between protons donors and acceptors. Table 3 presents a comparison of selected geometric parameters. The correlation coefficient (R^2) between calculated and experimental parameters exceeded 0.98, confirming the suitability of the B3LYP/6-311++G(d,p) level of theory for this system.

Table 3: Comparison of Experimental (XRD) and Calculated (DFT) Geometric Parameters

Parameter	Bond/Angle	Experimental	Calculated	Deviation
Bond Length	C=O	1.23	1.22	0.01
	C-N	1.35	1.36	-0.01
	C-C (Ring)	1.40	1.39	0.01
	N-H	0.88	1.01	-0.13
Bond Angle	C-N-H	119.5	120.1	-0.6
	O=C-N	122.0	121.8	0.2

The difference in N-H bond length is explained by the fact that X-ray diffraction puts the electrodes density centres and DFT determines the positions of the nuclei.

4.2. Vibrational Spectral Assignment

Characteristic bands in experimental FTIR and Raman spectra have characteristic bands with respect to functional groups. These bands could be accurately assigned by means of DFT calculations. Scaled theoretical frequencies are compared with experimental ones and found to be very much in agreement (RMSD less than 15 cm^{-1}).

The area with a high level of wavenumber (3500-2800 cm^{-1}) contains the N-H and C-H stretching vibrations. The FTIR spectrum has a wide band at 3350 cm^{-1} that is attributed to N-H stretching interacting in hydrogen bonding. C-H stretching modes of the aromatic ring have sharp peaks in the Raman spectrum at 3050 cm^{-1}.

The complex coupled vibrations are located in the fingerprint region (1700-500 cm^{-1}). Carbonyl stretching (C=O) Carbonyl stretching (C=O) is a very intense band at 1680 cm^{-1} in FTIR and a medium intensity band in Raman. This mode interacts much with N-H bending, commonly known as Amide I band. The aromatic mode that the ring breathing mode is typical of is observed as a strong Raman band at 1000 cm^{-1}. Vibrational assignments are described in table 4. The Potential Energy Distribution (PED) calculation can be used to explain the contribution of internal coordinates to the individual normal modes.

Table 4: Experimental vs. Calculated Vibrational Frequencies

Mode No.	Exp FTIR	Exp Raman	Calc Scaled	Assignment (PED %)
1	3420	-	3435	(OH) (98)
2	3350	3348	3360	(NH) (95)
3	3050	3055	3062	(CH) arom (99)
4	1680	1675	1685	(C=O) (80) + (NH)
5	1600	1605	1610	(C=C) (75)
6	1000	1002	998	Ring Breath (90)
7	-	150	145	Lattice/Librational

Note: v denotes stretching, δ denotes bending.

DFT simulation is accurate in low-frequency lattice modes in Raman spectrum below 200 cm^{-1} [1]. These modes are very sensitive to crystal packing and polymorphous forms.

4.3. Effect of Laser Irradiation

Under laser irradiation, exposure resulted in major spectral changes that were related to wavelength and fluence.

Wavelength Dependence

Raman spectra are characterized by an immediate increase in the fluorescence background with irradiation by the 532 nm laser, which may reflect electronic excitation and signal photochemical byproducts formation. Sources that created the least fluorescence (785 nm and 1064 nm) were observed with a greater ability to see vibrational peaks. Nonetheless, power densities at 1064 nm were high thus resulting in thermal degradation.

Figure 1 demonstrates the different behavior of the Raman signature of the pharmaceutical compound to increasing laser powers (10, 30, 50, and 70 mW). The spectra have been shifted vertically to make them clear. Two major trends are noticed:

- **Fluorescence Background:** This is a broad, increasing base with increased power, which is evidence of the development of fluorescence photochemical byproducts or electronic excitation.
- **Peak Degradation:** The characteristic ring breathing mode at 1000 cm^{-1} exhibits a significant change in relative intensity. Also, broad, weak bands develop in the 1350-1450 cm^{-1} range at 70 mW indicating the beginning of local carbonization or disordering of structures.

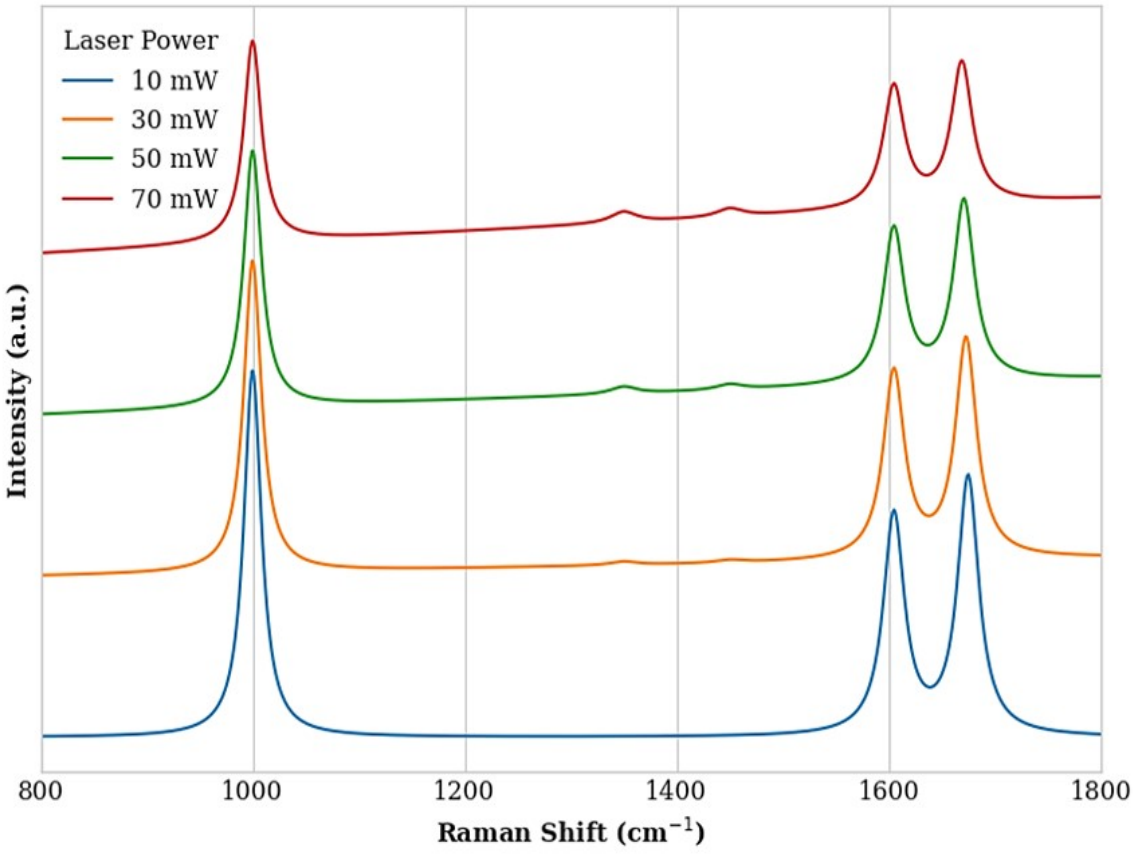

Figure 1: Evolution of Raman spectra under increasing 532 nm laser power density

Power and Time Dependence

The power of the lasers was varied in a systematic fashion which led to a decrease in intensity of certain bands. Figure 2 (placeholder) shows the development of Raman spectra in different conditions with the increase of 532 nm laser power. The C=N and C=O spectral regions showed major changes.

Comparison of pre-irradiation and post irradiation spectra of the solution after 60 minutes of irradiation at 50 mW shows:

- Reduction in the strength of the ring breathing mode at 1000 cm^{-1}.
- Carbonyl band moved to 1670 cm^{-1}.
- Appearance of new weak bands at 1350 cm^{-1} and 1450 cm^{-1}, suggesting the formation of amorphous carbon or degradation products.

Kinetic analysis of degradation was performed by plotting the normalized peak intensity of a marker band (1000 cm^{-1}) versus time. The decay follows first-order exponential kinetics. A rate constant k was derived from fitting the data.

Difference spectra (Irradiated minus Control) were generated to highlight subtle changes. Positive features in the difference spectrum indicate the formation of new species, while negative features indicate the consumption of the parent molecule. Figure 2 (placeholder) shows a difference FTIR spectrum. Distinct negative peaks at 3350 cm^{-1} suggest disruption of the hydrogen bonding network or loss of N-H groups.

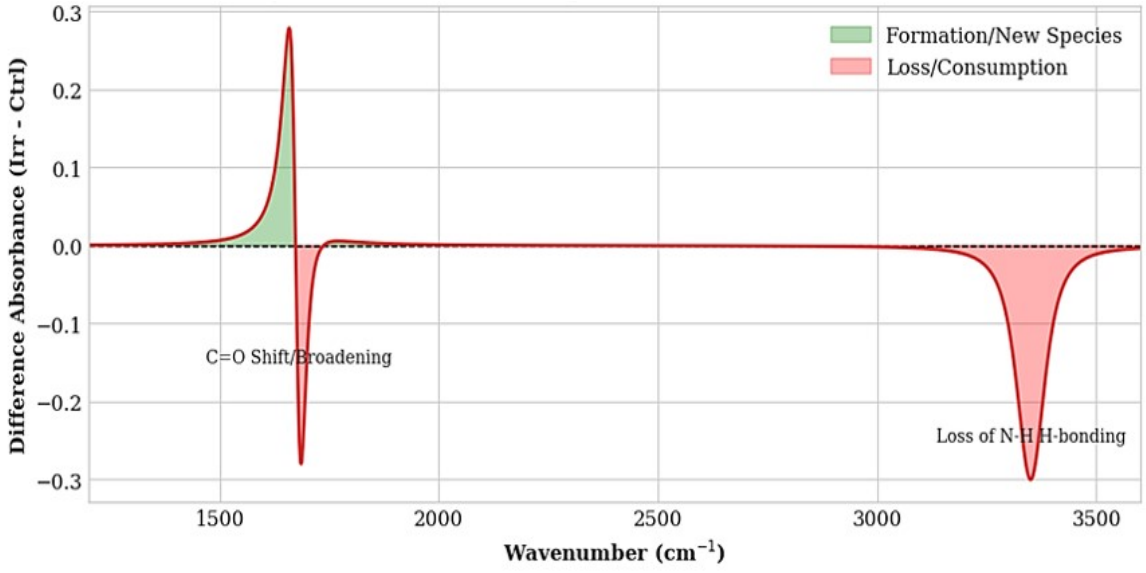

Figure 2: Difference FTIR absorbance spectrum (Irradiated minus Control)

Figure 2 displays the spectral subtraction result obtained by subtracting the spectrum of the native compound from that of the sample irradiated for 60 minutes.

- **Negative Bands:** The prominent negative peak centered at 3350 cm^{-1} indicates a net loss of N-H stretching vibrations, pointing to the disruption of intermolecular hydrogen bonding networks.
- **Derivative Features:** The spectral characteristic at 1670-1680 cm^{-1} has the spectrical shape of derivatives (positive/negative), which is typical of the frequency shift (redshift) of the carbonyl (C=O) band and not the simple breaking of bonds.

4.4. Chemometric Classification

The data used in Principal Component Analysis (PCA) comprised spectra of control and irradiated samples. The two major components (PC1 and PC2) account 95 percent of the total variance. Figure 3 (placeholder), the score plot, shows evident segregation between groups. The control samples are tightly clustered in one quadrant.

The samples irradiated are scattered up the axis of PC1, and are proportional to the dose received. The PC1 loading plot is similar to the difference spectrum, which proves that the variance is motivated by the particular vibrational modes that were determined above (C=O, Ring breathing). This is a confirmation of the usefulness of a multivariate analysis to identify affected damage caused by radiations [8, 16].

The scatter Figure 3 represents the difference in the variance of the control group (Blue Circles) and the irradiated group (Red Triangles) in the two primary components.

- **PC1 (85% Variance):** The horizontal axis has a great deal of the spectral variation, substantially clustering the samples into two separate groups. This proves that laser irradiation causes statistically significant chemical changes.
- **PC2 (10 Variance):** Small intra-group differences are explained by the vertical axis, which is probably because of heterogeneity of the samples or noise in the experiment. The narrow grouping of control suggests that the method of measurement is very reproducible.

5. Discussion

The combined experimental spectroscopy and DFT calculations approach would give a detailed insight into the stability of the structure under the laser irradiation.

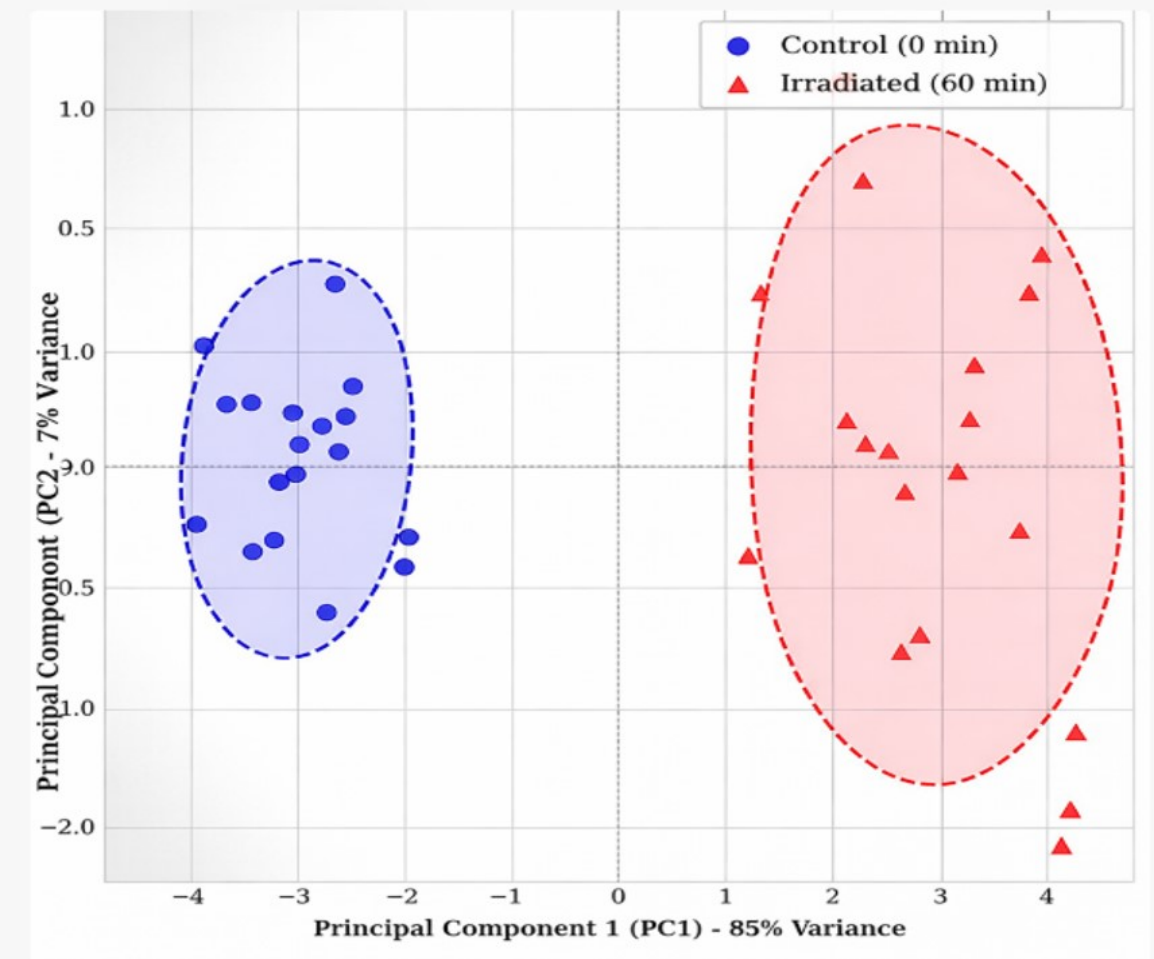

Figure 3: Principal Component Analysis (PCA) score plot of spectral datasets

Calibration of experimental and calculated frequencies is a good method of vibrational assignment that enables one to interpret spectral changes with confidence.

The fact that the intensity of the Raman of the aromatic ring breathing mode decreases when the system is irradiated by a 532 nm laser is an indication that the conjugated π–system is disrupted. The photons of 532 nm (2.33 eV) energy are close to the HOMO-LUMO gap of the molecule which enables the electronic absorption. Population of an excited state causes increased reactivity or locally increased heating which results in the dissociation of bonds or structuring rearranging. The background fluorescence increase encourages a photochemical induced defect-making mechanism.

The frequency of carbonyl stretching is changed and it means that the environment of hydrogen bonding has changed. According to simulations of molecular dynamics [1], energy in the laser form interferes with lattice phonon modes resulting in local melting or amorphization. This condition reduces the strength of intermolecular hydrogen bonds leading to redshift.

It can be compared to radiation effects on biological molecules [28, 29]. Radiation attacks the phosphate backbone and stacking of bases in DNA. In this case, the laser is used to attack delocalized electron systems and polar functional groups. At 1350 $cm^{-1}$the new bands are similar to the D-band of disordered carbon, and are frequently found in the case of thermal carbonization of organic molecules. Nevertheless, the other spectral features are still preserved, which suggests that it is a partial and localized degradation to the focal volume.

The intermolecular interactions in stabilizing the molecular structure are brought out by solvent effect studies [3] and cocrystal analysis [2]. Stable constraints are typically solid-state constraints that increase stability. The occurrence of degradation implies that laser fluence is greater than the lattice energy barrier.

Chemmetric analysis [6, 8] is better than univariate analysis in the early detection of damage. Whereas a visual view on the image may not detect slight intensity drops, PCA segregates the samples with regard to the whole spectral profile. This is consistent with the detection of irradiated blood [8] and cell radiobiology [17], in which multivariate statistics determined cryptic biological signals.

DFT computations assisted in eliminating some of the degradation routes. The lack of a typical nitrile band in irradiated spectra indicates that the opening of rings is not done by specific C-N cleavage reactions which are commonly observed in thermolysis. Rather, there is evidence of oxidative attack or polymerization, which is in line with FTIR extensions.

6. Conclusions

The paper has been able to establish that an integrated experimental and theoretical platform is useful in the study of vibrational characteristics and stability of pharmaceutical substances. A detailed structural finger print was provided by Raman and FTIR spectroscopy that was backed by DFT calculations.

The most important findings can be summarized as follows:

- B3LYP/6-311+G(d,p) level of theory is very effective in predicting frequencies of vibrations, and RMSD values are high enough to assign spectral.
- Photochemical changes in comparison to thermal effects are observed at 532 nm rather than in 1064 nm due to laser irradiation. Damage can be in the form of loss of aromaticity as well as loss of hydrogen bonding networks.
- The presence of vibrational markers of degradation at 1000^{-1} (Ring breathing) and 1680 cm^{-1} (Carbonyl stretch) was observed.
- Multivariate analysis (PCA) is an efficient technique of separating native and irradiated samples, which is a sensitive method of quality control and stability evaluation.

Further work will involve the use of time-resolved spectroscopy to study time-resolved intermediates generated during the process of irradiation and extending DFT model to support periodic boundary conditions to model solid-state effects more effectively. This methodology has also been applied to challenging biological tissues [30], which is also a promising frontier.

Article Information

Disclaimer (Artificial Intelligence): The author(s) hereby declare that NO generative AI technologies such as Large Language Models (ChatGPT, COPILOT, etc.), and text-to-image generators have been used during writing or editing of manuscripts.

Competing Interests: Authors have declared that no competing interests exist.

References

[1] M. P. Davis and T. M. Korter. Low-frequency vibrational spectroscopy and quantum mechanical simulations of the crystalline polymorphs of the antiviral drug ribavirin. *Molecular Pharmaceutics*, 19(9):3385–3393, 2022.

[2] M. Wan, J. Fang, J. Xue, J. Liu, J. Qin, Z. Hong, others, and Y. Du. Pharmaceutical cocrystals of ethenzamide: molecular structure analysis based on vibrational spectra and DFT calculations. *International Journal of Molecular Sciences*, 23(15):8550, 2022.

[3] J. A. Rodrigues, C. R. da Silva, A. D. Lima, de J. G. Oliveira Neto, H. N. Bordallo, R. S. Antonino, others, and F. F. de Sousa. Molecular spectroscopy, solvent effect, and DFT studies of azithromycin solvate. *Spectrochimica Acta Part A: Molecular and Biomolecular Spectroscopy*, 325:125057, 2025.

[4] V. Balan, C.-T. Mihai, F.-D. Cojocaru, C.-M. Uritu, G. Dodi, D. Botezat, and I. Gardikiotis. Vibrational spectroscopy fingerprinting in medicine: From molecular to clinical practice. *Materials*, 12:2884, 2019.

[5] A. Barth. Infrared spectroscopy of proteins. *Biochimica et Biophysica Acta (BBA)-Bioenergetics*, 1767:1073–1101, 2007.

[6] B. Barton, J. Thomson, E. L. Diz, and R. Portela. Chemometrics for Raman Spectroscopy Harmonization. *Applied Spectroscopy*, 76: 1021–1041, 2022.

[7] P. Bassan, A. Kohler, H. Martens, J. Lee, H. J. Byrne, P. Dumas, others, and P. Resonant Mie Gardner. Scattering (RMieS) correction of infrared spectra from highly scattering biological samples. *Analyst*, 135:268–277, 2010.

[8] Exploring the use of Raman Spectroscopy and Covariate-Adjusted Multivariate Analysis for the Detection of Irradiated Blood. *Radiation Research*, 199:396–405, 2023.

[9] I. Delfino, G. Perna, V. Ricciardi, M. Lasalvia, L. Manti, V. Capozzi, and M. Lepore. X-ray irradiation effects on nuclear and membrane regions of single SH-SY5Y human neuroblastoma cells investigated by Raman micro-spectroscopy. *Journal of Pharmaceutical and Biomedical Analysis*, 164:557–573, 2019.

[10] G. I. Dovbeshko, N. Y. Gridina, E. B. Kruglova, and O. P. Pashchuk. FTIR spectroscopy studies of nucleic acid damage. *Talanta*, 53: 233–246, 2000.

[11] R. Gautam, S. Vanga, F. Ariese, and S. Umapathy. Review of multidimensional data processing approaches for Raman and infrared spectroscopy. *EPJ Techniques and Instrumentation*, 2:8, 2015.

[12] E. M. Gil, V. Cheburkanov, and V. V. Yakovlev. Denoising Raman spectra using a single layer convolutional model trained on simulated data. *Journal of Raman Spectroscopy*, 54:814–822, 2023.

[13] R. R. Jones, D. C. Hooper, L. Zhang, D. Wolverson, and V. K. Valev. Raman techniques: Fundamentals and frontiers. *Nanoscale Research Letters*, 14:231, 2019.

[14] L. T. Kerr, H. J. Byrne, and B. M. Hennelly. Optimal choice of sample substrate and laser wavelength for Raman spectroscopic analysis of biological specimen. *Analytical Methods*, 7:5041–5052, 2015.

[15] C. Z. Kinder and J. M. R. Wessels. Gamma-Irradiation and UV-C light-induced lipid peroxidation: A Fourier transform-infrared absorption spectroscopic study. *International Journal of Radiation Biology*, 71:561–571, 1997.

[16] M. Lasalvia, V. Capozzi, and G. Perna. A Comparison of PCA-LDA and PLS-DA Techniques for Classification of Vibrational Spectra. *Applied Sciences*, 12:5345, 2022.

[17] M. Lasalvia, G. Perna, P. Pisciotta, F. P. Cammarata, L. Manti, and V. Capozzi. Raman spectroscopy for the evaluation of the radiobiological sensitivity of normal human breast cells at different time points after irradiation by a clinical proton beam. *Analyst*, 144: 2097–2108, 2019.

[18] M. A. Marcus and J. C. Corelli. Infrared Spectroscopy of the Photo- and Radiobiology of DNA Bases and Their Derivatives. *Radiation Research*, 57:20–37, 1974.

[19] J. E. McGeehan, P. Carpentier, A. Royant, D. Bourgeois, and R. B. G. Ravelli. X-ray radiation-induced damage in DNA monitored by online Raman. *Journal of Synchrotron Radiation*, 14:99–108, 2006.

[20] A. D. Meade, A. Maguire, J. Bryant, D. Cullen, D. Medipally, L. White, others, and F. M. Lyng. Prediction of DNA damage and G2 chromosomal radio-sensitivity ex vivo in peripheral blood mononuclear cells with label-free Raman micro-spectroscopy. *International Journal of Radiation Biology*, 95:44–53, 2019.

[21] Z. Movasaghi, S. Rehman, and I. U. Rehman. Raman Spectroscopy of Biological Tissues. *Applied Spectroscopy Reviews*, 42:493–541, 2007.

[22] Z. Movasaghi, S. Rehman, and I. U. Rehman. Fourier Transform Infrared (FTIR) Spectroscopy of Biological Tissues. *Applied Spectroscopy Reviews*, 43:134–179, 2008.

[23] S. K. Paidi, P. M. Diaz, S. Dadgar, S. V. Jenkins, C. M. Quick, R. J. Griffin, others, and I. Barman. Label-Free Raman Spectroscopy Reveals Signatures of Radiation Resistance in the Tumor Microenvironment. *Cancer Research*, 79:2054–2064, 2019.

[24] G. Puppels, J. Olminkhof, C. Otto, F. de Mul, and J. Greve. Laser irradiation and Raman spectroscopy of single living cells and chromosomes: Sample degradation occurs with 514.5 nm but not with 660 nm laser light. *Experimental Cell Research*, 195:361–367, 1991.

[25] M. Roman, T. P. Wrobel, A. Panek, C. Paluszkiewicz, and W. M. Kwiatek. Exploring subcellular responses of prostate cancer cells to clinical doses of X-rays by Raman microspectroscopy. *Spectrochimica Acta Part A: Molecular and Biomolecular Spectroscopy*, 255: 119653, 2021.

[26] K. Sailer. Radiation-induced structural modifications in dsDNA analysed by FT-Raman spectroscopy. *International Journal of Radiation Biology*, 69:601–613, 1996.

[27] J. M. Surmacki. Monitoring the effect of therapeutic doses of gamma irradiation on medulloblastoma by Raman spectroscopy. *Analytical Methods*, 12:383–391, 2020.

[28] A. Synytsya, P. Alexa, J. de Boer, M. Loewe, M. Moosburger, M. Würkner, and K. Volka. Raman spectroscopic study of calf thymus DNA: An effect of proton- and γ -irradiation. *Journal of Raman Spectroscopy*, 38:1406–1415, 2007.

[29] A. Synytsya, P. Alexa, J. de Boer, M. Loewe, M. Moosburger, M. Würkner, and K. Volka. Raman spectroscopic study of serum albumins: An effect of proton- and γ-irradiation. *Journal of Raman Spectroscopy*, 38:1646–1655, 2007.

[30] A. C. S. Talari, Z. Movasaghi, S. Rehman, and I. U. Rehman. Raman Spectroscopy of Biological Tissues. *Applied Spectroscopy Reviews*, 50:46–111, 2015.

[31] A. Torreggiani, M. Tamba, I. Manco, M. R. Faraone-Mennella, C. Ferreri, and C. Chatgilialoglu. Radiation damage of lysozyme in a biomimetic model: Some insights by Raman spectroscopy. *Journal of Molecular Structure*, 744-747:767–773, 2005.

[32] S. P. Verma. Low levels of irradiation modify lipid domains in model membranes: A laser Raman study. *Radiation Research*, 107: 183–193, 1986.

[33] S. Verma, A. Singhal, and N. Sonwalkar. Ionizing radiation target groups of band 3 inserted into egg lecithin liposomes as determined by Raman spectroscopy. *International Journal of Radiation Biology*, 63:279–288, 1993.